Modelling the static stiffness and dynamic frequency response characteristics of a leaf spring truck suspension

J B Hoyle
Alvis Vickers Limited, Hadley Castle Works, Telford, Shropshire TF1 6QW, UK

Abstract: The suspension characteristics of a 10 ton truck with a highly non-linear leaf spring suspension have been investigated. The acceleration transmissibility frequency response characteristics of the truck were first investigated. Results showed that whereas the bounce (sprung mass) resonant frequency was quite close to that expected, the wheel-hop (unsprung mass) resonant frequencies were roughly twice that expected. As no obvious mechanism for this effect was evident, the static stiffness characteristics of the suspension were measured in an attempt to understand this phenomenon. A simple plot of the resulting suspension-generated force against suspension deflection showed that two distinct stiffness regimes were present; the first, which was associated with small suspension deflections of between 2 and 4 mm, was significantly greater than the second, which was associated with larger suspension deflections.

A state-variable linear 5 degree-of-freedom spring mass damper model of the vehicle was created within MATLAB in an attempt to predict the frequency response characteristics of the vehicle. The state-variable model predictions were close to those seen experimentally for the sprung mass at frequencies below 3 Hz, but were quite incorrect for both the sprung and unsprung masses above this frequency. The state-variable model was then used again with increased values of suspension stiffness and results showed that using these higher values led to a more accurate predicted response for both the sprung and unsprung masses above 3 Hz, whereas below this frequency their responses were clearly incorrect. Comparison of experimental and predicted results showed that the vehicle frequency response was dominated above 3 Hz by the low suspension deflection–high stiffness regime identified in the static stiffness results, whereas below this frequency, the high suspension deflection–low stiffness regime tended to dominated the response.

To overcome the problem of the transition from the low to the high stiffness regimes when predicting the frequency response characteristics, a non-linear model was created using MATLAB and SIMULINK. Results showed that the model was able to capture this transition, with resulting frequency response curves for both the sprung and unsprung masses being very similar to the experimental results. Further refinements to the model were able to account for additional discrepancies between predictions and experimental results.

The non-linear nature of the spring stiffnesses, resulting in a very useful hysteresis damping effect at the sprung mass resonant frequency, meant that for most normal road conditions the vehicle would ride on a near solid suspension. The apparent advantages of the extra damping would therefore be offset by a significant decrease in ride quality, and this was especially evident in respect to road noise and vibration—a finding borne out in practice.

This paper establishes the principal characteristics of the truck suspension and goes on to describe the linear state-variable and non-linear models created to simulate the frequency response characteristics of the vehicle suspension.

Keywords: static stiffness, dynamic frequency response, leaf spring truck suspension

1 INTRODUCTION

Leaf spring suspensions can consist of a single leaf or multiple leaves in parallel. In the latter case, provided that the leaves are similar, the effective stiffness of the suspension can be considered to be the sum of the stiffnesses of the individual leaves.

One feature of leaf spring suspensions is their relatively large amount of inherent damping compared to other forms of suspension design. As a multileaf spring suspension deflects, the leaves must slide over one

The MS was received on 4 April 2003 and was accepted after revision for publication on 11 September 2003.

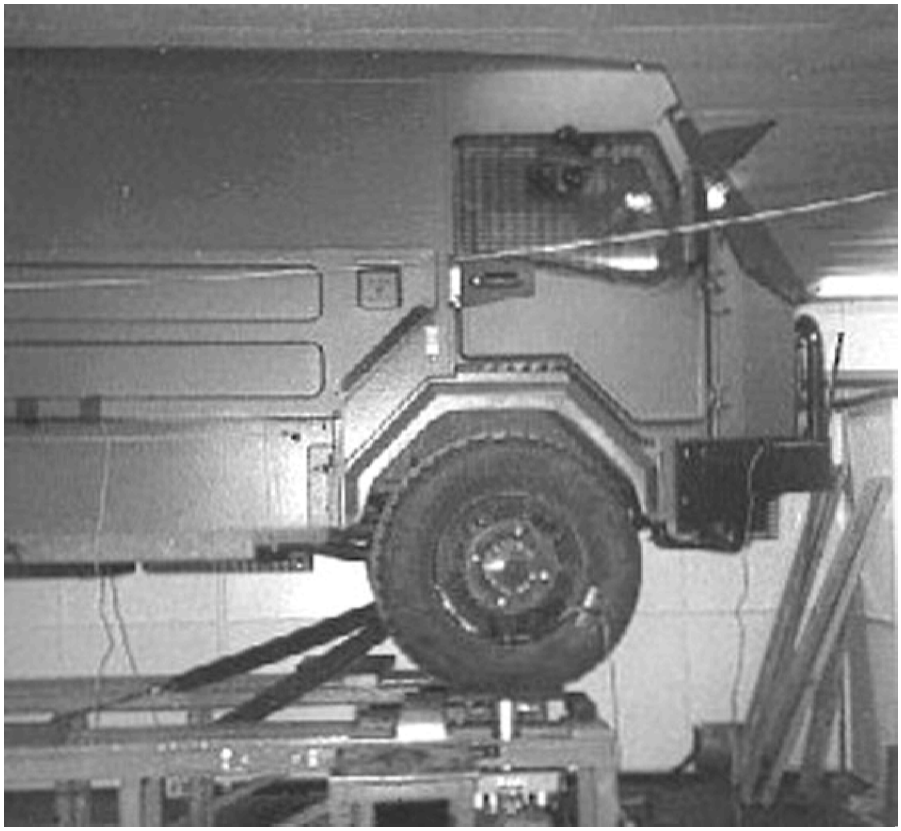

Fig. 1 Vehicle mounted on a four-post rig

another at some point along their length or else they would act like a solid beam. Due to friction between the leaves, the sliding of the leaves generates friction forces that resist further deflection of the suspension. This resistance to further deflection acts like normal damping in as much as it is direction dependent, but because it tends to be Coulombic in nature ('stiction'), it does not act like the viscous damping associated with normal shock absorbers. This form of Coulomb friction is not conducive to the creation of good ride characteristics for the vehicle because it is difficult to control.

For designs where a number of similar leaves are used in parallel, the leaves will all carry approximately the same load. This means that where the leaves are in contact, large friction forces will be generated when the suspension deflects and the leaves slide over one another. Furthermore, if a certain load has to be applied to the suspension in order to overcome the friction between the leaves, then until this load has been reached the leaves will act like a solid beam. Implicit in this scenario is the possibility that for small deflections the locked leaves will have a different, and probably higher, stiffness than the sum of the stiffnesses of the individual leaves.

The static stiffness of multileaf spring suspensions has been measured by various groups [**1**–**3**]. The various authors presented results which showed that, depending on the suspension design, the stiffness was highly nonlinear in the fashion described above. Different stiffness regimes were evident depending on the amplitude, and energy was lost into the suspension during cycling due to the hysteresis effects of Coulomb friction. Other results by the same authors showed that the Coulomb friction increased with load and deflection and that the hysteresis losses were independent of frequency.

2 TRUCK LEAF-SPRING SUSPENSION CHARACTERISTICS

Both the acceleration transmissibility frequency response characteristics and the static stiffness characteristics of a 10-ton truck with leaf-spring suspension have been investigated using a four-post rig. This rig, partly shown in Fig. 1, consisted of four servo-controlled hydraulic vertical-axis actuators with horizontal plates on the ends, one plate and actuator to support each wheel. The actuators incorporated displacement and load transducers, the former for position feedback control and the latter for load feedback control. Instrumentation was included that enabled frequency sweeps and data capture to be conducted, as was a computer for the analysis of the resulting data.

2.1 Dynamic results

The bounce (sprung mass) and wheel-hop (unsprung mass) acceleration transmissibility frequency responses

were derived from the four post rig. Sine wave displacements were input to the wheels via the actuators, their frequencies being increased in increments while the amplitude decreased similarly. Accelerometers mounted on the wheels, the vehicle body and the actuators enabled the acceleration transmissibility frequency responses to be generated.

2.1.1 *Acceleration transmissibility frequency responses*

The results from the transmissibility frequency response tests are shown in Fig. 2a (sprung mass) and Fig. 2b (unsprung masses). Figure 2a shows three curves, these being the response of the centre of gravity of the vehicle body (marked 'CG'), the front of the vehicle body (marked 'F') and of the rear (marked 'R'). Figure 2b shows four curves, one curve for each wheel. The two curves for the wheels on the front axle (marked 'F') were very similar, as were those for the wheels on the rear axle (marked 'R').

2.1.2 *Sprung and unsprung mass natural frequencies*

The bounce (sprung mass) resonant frequency and corresponding amplitude ratio of the centre of gravity of the vehicle body can be seen (in Fig. 2a) to have been 2.44 Hz and 10.24 dB respectively, with the natural frequency of the front of the vehicle being slightly lower and that of the rear being slightly higher. This indicated that although the vehicle body responded mainly in bounce, there was a slight amount of pitch evident, with the slightly higher natural frequency and lower amplitude of the rear reflecting the slightly stiffer suspension and greater damping (effects of the assistor springs).

The wheel hop (unsprung mass) resonant frequency and amplitude ratio can be seen (see Fig. 2b) to have been about 19 Hz and 1 dB respectively, with both front wheels being very similar to the rear wheels.

2.1.3 *Predicted natural frequencies*

Approximate values for the undamped natural frequencies of the sprung and unsprung masses can be predicted using standard techniques [**4**]. These techniques assume that the vehicle can be modelled as a simple linear 2 degree-of-freedom (DoF) system. This is a reasonable assumption considering that the unsprung natural frequencies were very similar and that the vehicle body experienced very little pitch in the primary bounce mode. For an undamped linear 2 DoF system, the predicted sprung (ω_s) and unsprung (ω_{us}) resonant frequencies are given by

$$\omega_s = 1/2\pi\sqrt{K_s K_t/[M_s(K_s + K_t)]} \quad \text{Hz} \tag{1}$$

$$\omega_{us} = 1/2\pi\sqrt{(K_s + K_t)/M_{us}} \quad \text{Hz} \tag{2}$$

where M_s is the sprung (vehicle body) mass, M_{us} is the sum of the two unsprung masses (front and rear axles with wheels), K_s is the sum of the front and rear suspension stiffnesses and K_t is the sum of the front and rear tyre stiffnesses. Substitution of experimentally measured values into these equations [8210 kg ($M_b - M_e$), 1300 kg ($M_f + M_r$), 1.74 MN/m ($K_{Lowf} + K_{Lowr}$) and 4.28 MN/m ($2K_t$) respectively (see Table 1)] give predictions for the bounce (sprung mass) and wheel-hop (unsprung mass) natural frequencies as 1.95 and 10.8 Hz respectively. Whereas the bounce natural frequency prediction was close to that measured experimentally on the actual vehicle (2.44 Hz), the wheel-hop natural frequency was not. The latter, at 19 Hz, was roughly twice that predicted by equation (2). It is in response to these discrepancies that further experimental and indeed theoretical investigations were carried out.

2.2 Static stiffness results

In an attempt to determine the reason for these unusual frequency response characteristics, the static stiffnesses

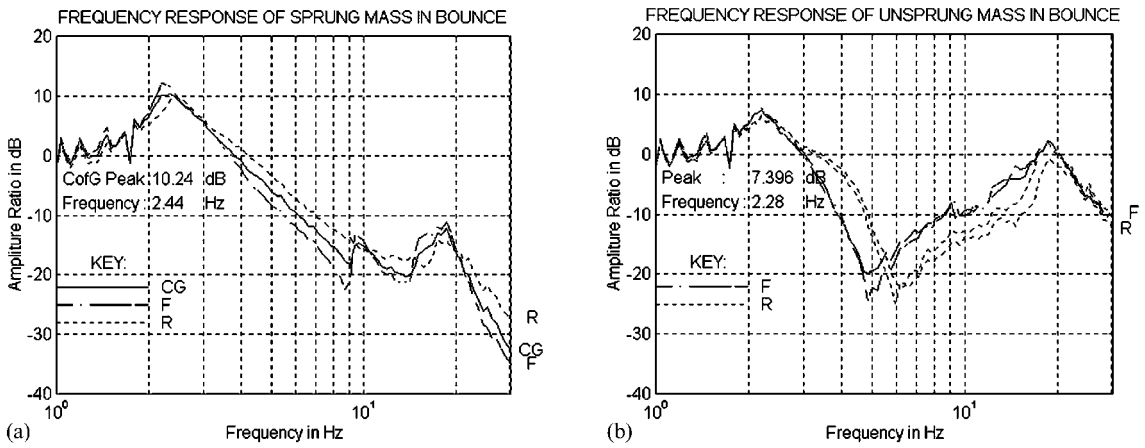

Fig. 2 (a) Experimental sprung mass frequency responses and (b) experimental unsprung mass frequency responses

Table 1 Look-up table of data used in the model

Symbol	Vehicle parameter	Source	Value
C_e	Damping of engine mounts	Estimated	2.28 kN s/m
C_f and C_r	Linearized front shock absorber damping for 5 DoF state-variable model; value based on manufacturer's damper data	Calculated	20 kN s/m
I_b	Pitch moment of inertia of vehicle body; derived from $M_b(L_{fr}/2)^2$ and rounded to nearest whole thousand	Calculated	23 000 kg m^2
K_{asrr}	Stiffness of assistor spring relaxation and recovery element	Estimated	80 kN/m
K_{ax}	Stiffness of axle stand	Estimated	10.0 MN/m
K_c	A constant defining the velocity input to the friction plates in the leaf-spring model		
K_e	Stiffness of engine mounts (total stiffness)	Estimated	1.3 MN/m
K_{Highf}	Total 'locked leaf' stiffness of front suspension (sum of left and right springs)	Measured	4.82 MN/m
K_{Highr}	Total 'locked leaf' stiffness of rear suspension (sum of left and right springs)	Measured	5.04 MN/m
K_{Lowf}	Total nominal stiffness of front suspension (sum of left and right springs)	Measured	850 kN/m
K_{Lowr}	Total nominal stiffness of rear suspension (sum of left and right springs)	Mesured	890 kN/m
K_{st}	Stiffness of tie-down strop	Estimated	5.0 MN/m
K_t	Total stiffness of two tyres in parallel (front two tyres being identical to the rear two)	Measured	2.14 MN/m
L_{accelf}	Distance from body CG to front body mounted measurement accelerometer	Measured	2.83 m
L_{accelr}	Distance from body CG to front body mounted measurement accelerometer	Measured	−2.75 m
L_{ax}	Distance from body CG to axle stand (front and rear)	Measured	2.57 m and −1.70 m
L_e	Distance from body CG to engine CG and mountings	Measured	1.70 m
L_f	Distance from body CG to front axle	Measured	1.574
L_{fr}	Wheel base	Measured	3.3 m
L_r	Distance from body CG to rear axle	Measured	−1.726 m
L_{st}	Distance from body CG to tie-down strop (front and rear)	Measured	2.83 m and −2.72 m
M_b	Body (sprung) mass	Measured	8610 kg
M_e	Mass of engine	Estimated	400 kg
M_f	Mass of front axle (unsprung mass)	Estimated	700 kg
M_r	Mass of rear axle (unsprung mass)	Estimated	600 kg
$y_b, \dot{y}_b, \ddot{y}_b$	Vertical displacement, velocity and acceleration of vehicle body		
$y_e, \dot{y}_e, \ddot{y}_e$	Vertical displacement, velocity and acceleration of engine		
$y_f, \dot{y}_f, \ddot{y}_f$	Vertical displacement, velocity and acceleration of front axle		
$y_r, \dot{y}_r, \ddot{y}_r$	Vertical displacement, velocity and acceleration of rear axle		
$Y_1, \dot{Y}_1$	Suspension displacement and velocity input into the leaf-spring model and assistor-spring model		
Y_2	Displacement of the friction plates in the spring-model		
Y_3	Displacement of relaxation and recovery element in the leaf-spring model		
Y_4	Nominal deflection of the rubber assistor spring		
Y_5	Deflection of relaxation and recovery element in the assistor-spring model		
μ_f	Effective coefficient of friction of front suspension leaves	Measured	0.09
μ_r	Effective coefficient of friction of rear suspension leaves	Measured	0.12
$\Theta_b, \dot{\Theta}_b, \ddot{\Theta}_b$	Pitch angular displacement, velocity and acceleration of vehicle body		

of the suspension were measured. This was achieved by tying the vehicle chassis down to the actuator bed plate and jacking up the actuators under the wheels. Separate displacement transducers were used to measure the suspension deflection of the axles relative to the vehicle body, and the load transducers in the actuator heads were used to measure the resulting reaction at the tyre-to-ground contact. Load versus deflection curves were thus generated for the suspension, and all these curves included a load offset due to the static weight of the vehicle.

The results that were obtained are shown in Figs 3 and 4, where Figs 3a and 4a are the plots of suspension-generated load (actually the tyre-to-ground contact force) against suspension deflection (axle movement relative to the vehicle body) and Figs 3b and 4b are the time histories of the suspension-generated load, deflection of the suspension and the velocity of the suspension deflection (axle velocity relative to vehicle body velocity). Figures 3 and 4 are for the front right and rear right suspensions respectively and are typical of the left sides.

2.2.1 *Stiffness characteristics*

The dynamic characteristics of the vehicle are generally determined by the stiffness and damping characteristics of the suspension, and the sprung and unsprung masses. Measuring the dynamic characteristics of the suspension is difficult due to the large number of variables involved. However, measuring the static characteristics is more

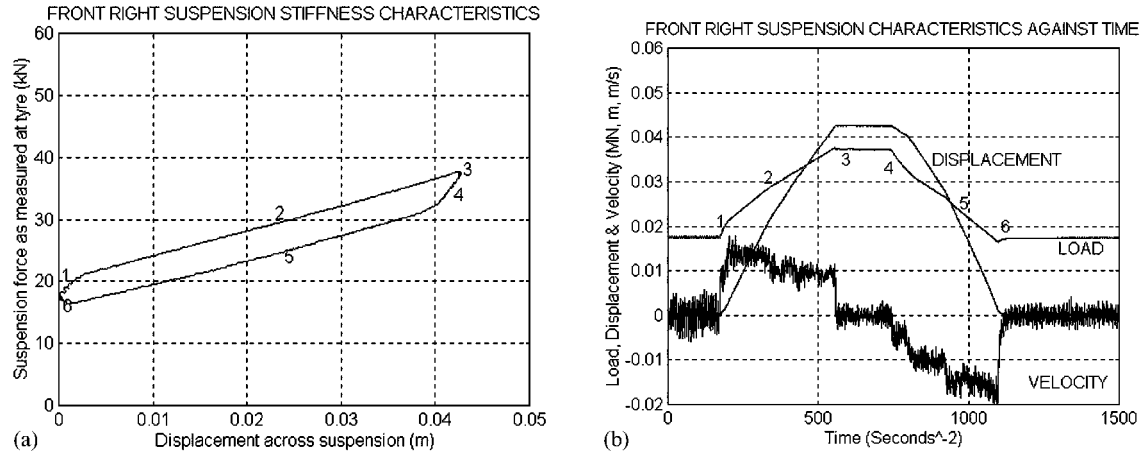

Fig. 3 (a) Experimental front static suspension stiffness and (b) experimental front stiffness time histories

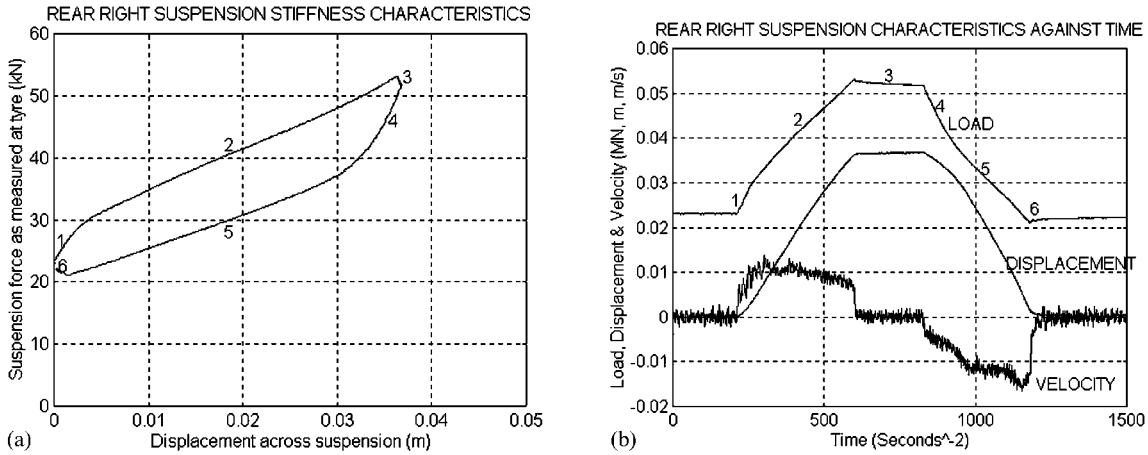

Fig. 4 (a) Experimental rear static suspension stiffness and (b) experimental rear stiffness time histories

straightforward and can generate useful information for the creation of models of such suspensions.

In the plots of generated load against suspension displacement (Figs 3a and 4a) for this vehicle, six different regimes were identified, these being numbered 1 to 6. The curves were non-linear and two distinct stiffnesses were evident in the stiffness characteristics. Regimes 1 and 4 were associated with the suspension leaves when they were in their locked state due to friction, the leaves acting like a solid beam to produce a stiffness that was much higher than the sum of the stiffnesses of the individual leaves. Regime 1 was generated at the initiation of increased suspension deflection as the already statically loaded suspension was further loaded, whereas regime 4 was generated at the initiation of suspension recovery as the greater-than-statically-loaded suspension was subsequently unloaded.

Regimes 2 and 5 were associated with the suspension leaves when they had broken free from their locked-up state and exhibited stiffnesses that were close to those expected from the sum of the stiffnesses of the individual leaves. Regime 2 was for the time when the suspension was loaded up and regime 5 was for the subsequent unloading of the suspension.

2.2.2 *Rubber bush relaxation*

When the suspension was held at a constant deflection for the period of time after a change in deflection had occurred, two more regimes were identified (regimes 3 and 6). When the suspension was loaded up and then held, the generated load at the tyre-to-ground contact dropped off slightly. Similarly, when the suspension was subsequently unloaded and then held, the generated load increased slightly. This phenomenon was assumed to be due to relaxation and recovery of the numerous rubber bushes that were incorporated in the suspension.

2.2.3 *Rubber assistor springs*

Although nominally identical, for deflections greater than those of static equilibrium, the rear suspension displayed a considerably higher stiffness than did the front, with also more relaxation and recovery of the suspension load when it was held at a constant deflection. This was due to the rear suspension having rubber assistor springs in parallel with the normal leaf springs. These assistor springs were fitted in such a way that they just contacted the axle at the normal ride height of the vehicle, and thus only assisted the leaf springs for deflections greater

than those caused by the static loads in the suspension. The relaxation and recovery effects of these assistor springs can be clearly seen in a comparison of regimes 3 and 6 in Figs 3a and 4a.

2.2.4 *Suspension stiffness values*

The nominal stiffness of the leaf springs was quoted by the manufacturer as 480 kN/m (120 kN/m per leaf), there being four identical leaf spring assemblies on the vehicle. If the loading and unloading regimes (regimes 2 and 5) are considered for the front suspension, the average of these gives a nominal stiffness for the suspension of 410 kN/m, considerably less than quoted by the manufacturer.

The same could not be measured directly for the rear suspension because of the inclusion of the rubber assistor springs. However, the manufacturer's quoted stiffness for the assistor springs was 0.15 MN/m. This value can be subtracted from the loading and unloading portions of the rear suspension stiffness curves, and the results of this exercise are shown in Table 2 (bracketed values being without the effects of the assistor springs). The average of the loading and unloading regimes (regimes 2 and 5) can thus be calculated, and at 460 kN/m is much closer to the manufacturer's quoted stiffness.

The stiffness of the leaf springs in regime 2 (loading) was higher than in regime 5 (unloading). The differences between these stiffness regimes can be accounted for by the fact that the friction between the leaves was proportional to the load being carried by the spring. As this load was increased, so too was the load required to overcome the friction between the leaves and unlock them. Thus the difference between the curves on the load against displacement plots at any one suspension deflection should have been greater at the higher loads than at the lower loads. This effect, resulting in a difference in the slopes (stiffness) of the curves, was just about detectable in the front suspension, but was rather more evident in the rear suspension (compare regimes 2 and 5 in Table 2).

The rows marked 'breakaway force loading' and 'breakaway force unloading' in Table 2, referring to the loading and unloading parts of the curves respectively, represent the changes in the suspension loads from a static state that were required to break the suspension springs free from their locked states. These values were derived from regimes 1 and 4 in the curves shown in Figs 3a and 4a. These 'breakaway' loads must in some way be related to the coefficient of friction between the leaves and the load carried by the suspension. A value that is related to the coefficient of friction between the leaves could thus be derived, and is shown in the last row in Table 2.

The coefficients of friction derived were low compared to normal steel to steel friction, but this was due to the large mechanical disadvantage under which the friction acted. The higher stiffness beam was only created by the inter-leaf friction preventing the leaves sliding relative to one another at their outer ends. As the leaves were nominally straight and near-horizontal in the statically loaded condition, the unsupported centre of the leaves was able to move significantly further in the vertical direction than could the supported outer ends in the horizontal direction. This meant that even a high inter-leaf coefficient of friction preventing the ends of the leaves from moving horizontally relative to one another translated into only a small effective coefficient of friction preventing the centre of the leaves from moving in the vertical direction, and it is this latter value that has been measured directly in the static stiffness results and appears in Table 2.

The stiffness of regimes 1 and 4 when the suspension leaves were locked together to form a solid beam can also be seen in Table 2. These stiffnesses were all greater than those of regimes 2 and 5. Table 3 shows the averaged stiffnesses for these regimes (averages of regimes 1 and 4 and of 2 and 5, for both front and rear suspensions). The values for the stiffnesses of the rear suspension springs in regimes 1 and 4 (bracketed values in Table 2) were obtained, as described above, by subtracting the assistor spring nominal stiffness (the value of the relatively linear portion below deflections of 40 mm of the assistor spring) from the measured suspension stiffnesses.

These stiffness characteristics were further analysed to give the ratio between these low and high stiffness regimes (the average of regimes 1 and 4 compared to the average of regimes 2 and 5). These are also shown in

Table 2 Suspension stiffness characteristics

Spring	Front right	Rear right	Rear right bump spring
Stiffness (MN/m)			
Regime 1	1.60	2.30 (2.15)	0.15
Regime 2	0.42	0.67 (0.52)	0.15
Regime 4	3.00	3.08 (2.93)	0.15
Regime 5	0.40	0.55 (0.40)	0.15
Break away force (KN)			
Loading	4.0	5.5	
Unloading	5.5	13.0	
Effective coefficient of friction	0.09	0.12	

Table 3 Consolidated stiffness characteristics

Spring position	Front right suspension	Rear right suspension
Averaged low stiffness (regimes 2 and 5)	0.41 MN/m	0.46 MN/m
Averaged high stiffness (regimes 1 and 4)	2.30 MN/m	2.54 MN/m
Stiffness ratio	5.61	5.52

Table 3, the stiffness ratio for the front being very similar to that of the rear.

It is evident that the suspension exhibited two different stiffness regimes, which were the nominal stiffness expected from the sum of the individual leaves and a higher stiffness that was a result of the leaves locking together to form a solid beam of some form. The resulting stiffness characteristics would have a definite energy absorbing capability (damping) once the leaves had broken free from their locked-up state. The amount of energy dissipated into the suspension would be proportional to the area of the loop in the load against deflection curves, which would produce a contribution to the overall damping in the suspension.

The stiffness characteristics of the assistor springs were obtained from the manufacturer. They were of the bellow type and acted as a bump spring only in the extremes of deflection ('bellow bound'!). During test, they had been subjected to a sine wave displacement with an amplitude of 0.0295 mm and a frequency of 2 Hz, the assistor spring being kept in contact with the actuator over the whole stroke. The load versus deflection characteristics for these assistor springs are shown as the curve originating and terminating at the origin in Fig. 5. This curve shows that the assistor springs exhibited hysteresis-type behaviour, in that a characteristic loop was evident. The stiffness of the assistor spring was found by taking the average of the loading and unloading portions of the loop over the lower half of the deflection range. For low deflections of less than 40 mm, the springs had a stiffness of about 0.15 MN/m.

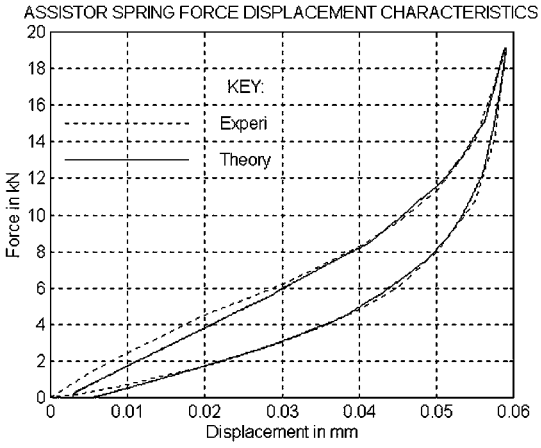

Fig. 5 Assistor spring stiffness characteristics

3 LINEAR 5 DoF STATE-VARIABLE MODEL

Having measured the frequency response of the vehicle and its static stiffness characteristics, an attempt was made to predict the frequency responses of the vehicle using a linear 5 DoF state-variable model within MATLAB. The model and its predictions are given in full in the Appendix.

When using the nominal stiffnesses (lower values) of the leaf springs, the linear 5 DoF state-variable model was able to predict the resonant frequency of only the sprung mass with any reasonable accuracy (1.8 Hz predicted compared to 2.44 Hz). Furthermore, the predicted sprung mass amplitude ratio (13.5 dB) at this frequency was greater than that seen experimentally (about 10 dB). Above this frequency the predictions completely failed to match the experimental behaviour of either the sprung or unsprung masses (compare Figs 1a and b with Figs 20a and b in the Appendix respectively).

A much better prediction for the sprung and unsprung masses was obtained using the higher stiffness values of the locked-leaf suspension, but again this was only true for frequencies above 3 Hz (compare Figs 2a and b with Figs 21a and b in the Appendix respectively). Below this frequency, the linear model predictions again completely failed to match the experimental results. The close match between the linear state-variable model and the experimental results above 3 Hz indicated that above this frequency the response of the vehicle was dominated by the higher locked-leaf state of the leaf springs, at least for the amplitudes of excitation used during these tests.

It was clear that the linear model was unable to simulate the transition from the high deflection–low stiffness regime of the leaf springs to the low deflection–high stiffness regime when making predictions for the frequency responses. It was for this reason that a significantly more complex non-linear model was created using MATLAB and SIMULINK.

4 NON-LINEAR 5 DoF MODEL

The unusual frequency response behaviour of the vehicle and subsequently identified low and high stiffness regimes in the static stiffness measurement results, together with the failure of the linear state-variable model to accurately predict the frequency response over the full frequency range, indicated where the emphasis was to be placed during the creation of the non-linear model. There were three component parts to the suspension that deserved special attention: the leaf springs (section 4.1), the rubber assistor springs (section 4.2) and the shock absorbers (viscous dampers) (section 4.3). The models for these are developed separately, with all notation and values being given in Table 1 and Fig. 6.

4.1 Leaf-spring model

Various methods by which the non-linear stiffness and friction characteristics of leaf-spring suspensions can be modelled are available [**3**, **4**]. The method adopted here is described below. As there were two relatively clearly

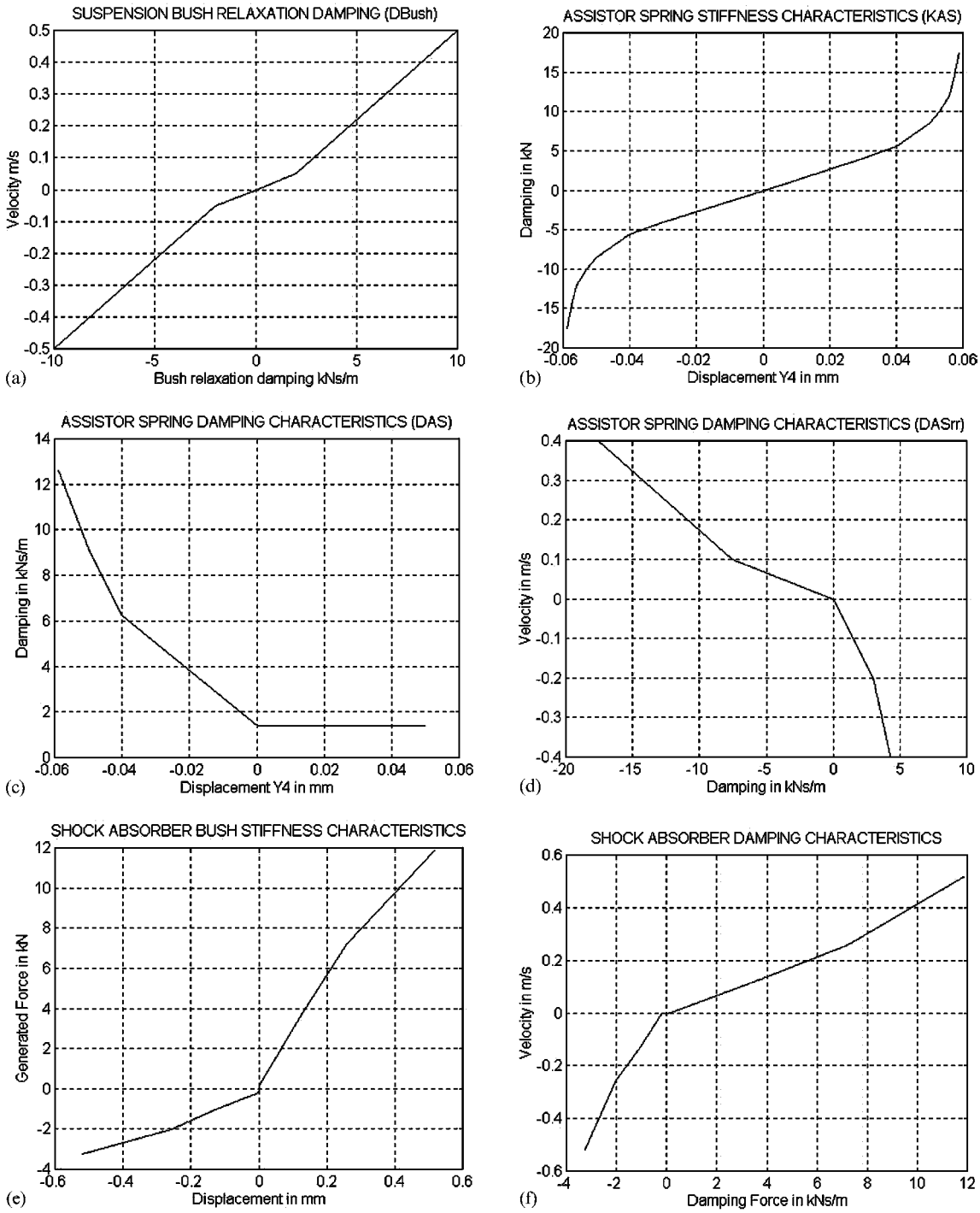

Fig. 6 Suspension leaf bush, assistor spring and shock absorber characteristics

delineated stiffness regimes, it was anticipated that a suspension model that had two springs in series, with some kind of friction model between the two, might suffice, as shown in the right-hand half of Fig. 7. The friction device would consist of friction plates with a load acting on them in such a manner as to push them together. This load, P in Fig. 7, was assumed to be proportional to the load generated by the nominal stiffness element of the suspension, K_{Low}, but it would be the load generated by the higher stiffness element of the suspension, K_{High}, that would act on the axle and therefore react on the vehicle body. The load P was assumed to be non-zero for all suspension deflections other than that of the completely unloaded condition (unladen free length of spring).

One of the friction plates was fixed to the vehicle body. The friction plate attached between the low and high stiffness springs slides relative to this body-mounted

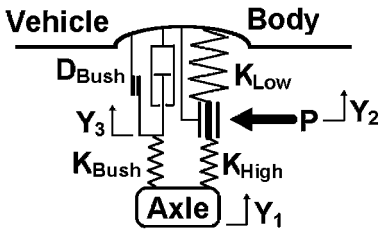

Fig. 7 Leaf-spring suspension model

plate only when the high stiffness spring had been compressed or extended sufficiently to overcome the friction loads generated by the plates and the resistive loads generated by the low stiffness spring. Thus for small deflections of the statically preloaded suspension, the stiffness would generally be that of the high stiffness spring, because the friction plate would not slide relative to the vehicle body. For larger deflections, the load generated by the high stiffness spring would be sufficient to overcome the friction and resistive loads generated by the plates and low stiffness spring, and thus force the plates to slide relative to one another. In these circumstances, the stiffness characteristics would be largely governed by the low stiffness element of the suspension. The resistive forces produced by the friction plates would be proportional to a load P acting on the plates and the coefficient of friction between the plates, and would always act to oppose the axle motion relative to the vehicle body.

The other element of the leaf-spring model was the relaxation and recovery regimes generated by the use of rubber bushes in the suspension. This element was modelled as a spring in series with a damper/Coulomb friction element, as shown in the left-hand half of Fig. 7. The stiffness of the bush and the damping/Coulomb friction element (the two in series allowing a degree of relaxation and recovery in the suspension) are denoted by K_{Bush} and D_{Bush} respectively and were modelled in parallel with the main suspension stiffness element to generate only the relaxation and recovery effect.

4.1.1 *Leaf-spring suspension governing equations*

The equations governing the force output from the leaf-spring suspension model are developed below. The inputs into the model were the deflection and velocity across the suspension, Y_1 and $\dot{Y}_1$ respectively, which are derived from the relative motions of the axles and vehicle body.

Leaf-spring suspension non-linear stiffness characteristics. The force on the vehicle generated by the suspension, F_{susp}, was made up of two components, these being the force generated by the high and low stiffness elements and that generated by the relaxation and recovery element, F_{k} and F_{rr}, respectively. Thus:

$$F_{\text{susp}} = F_{\text{k}} + F_{\text{rr}} \tag{3}$$

Considering the high and low stiffness elements,

$$F_{\text{k}} = (Y_1 - Y_2)K_{\text{High}} \tag{4}$$

where the deflection of the low stiffness element, K_{Low}, was denoted by Y_2. However, this force was resisted by the forces generated by the force P acting on the friction plates and the reaction of the low stiffness element. The sum of the resistive forces, F_{resist}, was given by

$$F_{\text{resist}} = -(Y_2 K_{\text{Low}}) \pm (\mu P) \tag{5}$$

where μ was the effective coefficient of friction between the friction plates. The force P was defined as

$$P = -(Y_2 K_{\text{Low}}) + P_0 \tag{6}$$

where P_0 was the preload at the zero suspension load (the free length of spring). Load P was assumed to be generated by the low stiffness element as it was the gross (large) deflections of the springs that produced the supportive loads that carried the weight of the vehicle, and the high stiffness elements were only created by the leaves locking together in the static condition when this load was exerted by the springs. The resistive forces therefore become

$$F_{\text{resist}} = -(1 \pm \mu)K_{\text{Low}} Y_2 \tag{7}$$

where P_0 was assumed to be zero. The direction of the friction forces was given by the $\pm$ sign in equation (7), such that the friction forces always opposed the direction of deflection of the suspension.

When the suspension was in the locked state with the leaves acting like a solid beam, the forces generated by the high and low stiffness elements of the suspension were given by equation (4), where Y_2 remained constant. However, when the leaves became unlocked and slipped relative to one another, the force generated by these springs was still given by equation (4), but the deflection Y_2 did not remain constant. This displacement, Y_2, was derived by integration of a component of the input velocity $\dot{Y}_1$.

These suspension characteristics were implemented in the model with the use of logic operators.

Leaf-spring suspension relaxation and recovery characteristics. The forces generated by the relaxation and recovery element in the suspension, F_{rr} in equation (3), were given by

$$F_{\text{rr}} = (Y_1 - Y_3)K_{\text{Bush}} \tag{8}$$

How this spring in series with a damper was implemented in the model is described below.

4.1.2 *Model implementation*

The model of the leaf springs was split into two distinct parts: that dealing with the non-linear stiffness characteristics and that dealing with the relaxation and recovery characteristics.

Leaf-spring suspension non-linear stiffness characteristics. The block diagram for the implementation of the non-linear stiffness characteristics is shown in Fig. 8. The inputs to the model were the relative deflection, Y_1, and the relative velocity, $\dot{Y}_1$, across the suspension.

The suspension deflection was first compared to the displacement of the slider, or friction plate, Y_2, to calculate the force in the high stiffness spring [equation (4)]. This force was then compared to the resistive forces created in both directions by the friction plates (friction coefficient of μ) and the low stiffness spring.

If the high stiffness force was greater than the higher limit, or less than the lower limit, then the 'logic operator' blocks returned a value of 1 (logical true) to switch 1. If the inputs to input 2 of either of the switch blocks exceeded their respective thresholds (both set to 0.5), then the switches would pass through their input 1. If it did not exceed their thresholds, they would pass through their input 3. If the input threshold (input 2) of switch 2 was exceeded by the output from switch 1 (the latter being the state of the logic operators), it would pass through a component of the suspension velocity to the integrator, which in turn would then derive the deflection of the friction plates, Y_2.

The velocity passed to the integrator was not the absolute velocity across the suspension, but a component of the velocity in proportion to the respective stiffnesses of the in-series low and high stiffness springs. The component was given by the constant K_c, where

$$K_c = \frac{K_{High}}{K_{High} + K_{Low}} \tag{9}$$

with the velocity being passed to the integrator always being less in absolute terms than the velocity across the suspension, $\dot{Y}_1$. The constant labelled 'preload' [P_0 in equation (6)] was set to zero. A non-zero constant here would create a friction force even when the force created by the low stiffness spring was zero. Switch 1 and the 'sign' block, the latter returning a 1 or -1 depending on the sign (direction) of its input velocity (relative velocities of the axle and vehicle body), were not strictly needed as far as the logic was concerned, but inclusion of these made the implementation of the model much more stable.

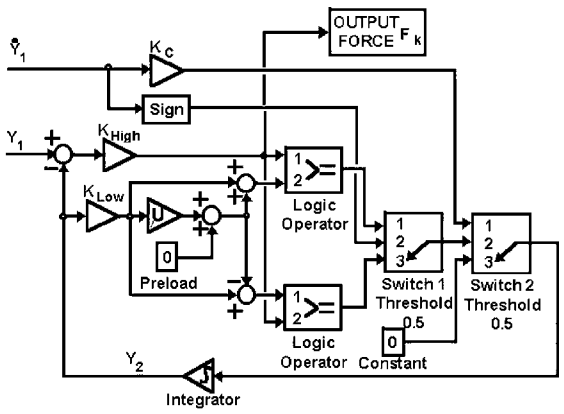

Fig. 8 Spring element block diagram

Leaf-spring suspension relaxation and recovery characteristics. The block diagram for the implementation of the relaxation and recovery element of the leaf springs is shown in Fig. 9. The input into the model was the deflection, Y_1, across the suspension. This was compared to the deflection of the damper, Y_3, and the resultant deflection of the spring, of stiffness K_{Bush}, was used to find the force acting on the damper [equation (8)]. As this type of model was always in a state of equilibrium (because there was no inertial mass associated with it), the force generated by the spring would always equal that developed by the damper. Thus the spring force was divided by the damping in order to derive the velocity of the damper. This velocity, $\dot{Y}_3$, was then integrated to derive the displacement of the damper.

A linear version of this system was tested against the normal transfer function representation of this type of model, to demonstrate that it worked. The advantage of the implementation presented here was that non-linear stiffnesses and damping could be incorporated in the model by replacing the linear gain blocks by look-up tables. Indeed, the damping included a Coulomb-like friction element as well as a viscous damping element, as shown in Fig. 7. The viscous damper element was needed to derive a meaningful velocity; i.e. the velocity had to be in some way proportional to the generated force. Failure to do this would result in a highly unstable model. The velocity–force relationship of the damper/Coulombic friction element is shown in Fig. 6a.

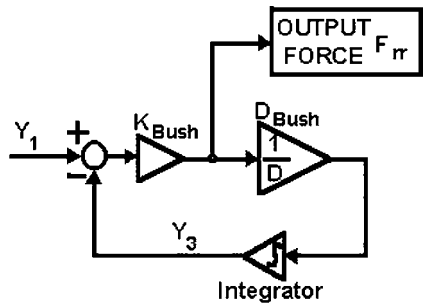

Fig. 9 Relaxation and recovery element block diagram

4.2 Rubber assistor springs

As noted previously, the rubber assistor springs were only included in the rear suspension, and even then only acted for suspension deflections beyond the static deflection of the springs. A spring and damper model was designed based on the available stiffness data and had approximately the right characteristics over the range of deflections of interest. This model is shown in Fig. 10, and is based on a spring K_{AS} in parallel with a damper D_{AS}, the characteristics of which are shown in Figs 6b

and c respectively. The model so far described, that of a spring in parallel with a damper, would not produce any appreciable relaxation and recovery effects. For this latter effect, a relaxation and recovery component was included by having a spring K_{ASrr} in series with a damper D_{ASrr}, the characteristics of which are shown in Fig. 6d, this combination being in parallel with the spring and damper described above K_{ASrr}.

The spring element K_{AS} would largely dictate the stiffness characteristics of the assistor spring, whereas the damper element D_{AS} would largely dictate the hysteresis characteristics. For completion, a non-linear spring of high stiffness was included, K_{AShigh}.

The assistor springs were manufactured as a reinforced rubber moulding and exhibited typical characteristics for components made from this material [**5**]. Other reinforced rubber components, such as automotive tyres, have been similarly modelled as springs in parallel with dampers [**6**], which is the approach developed here.

4.2.1 Governing equations

The equations governing the output from the rubber assistor springs are developed below. The input into the model was the deflection across the suspension, Y_1. This was compared to the nominal displacement of the assistor spring, Y_4, to find the force developed by the spring, K_{AShigh}. This was achieved with the aid of a look-up table, the resulting force, F_{AS}, being that which was developed by the assistor spring on the axle and vehicle body. K_{AShigh} was non-linear and generated zero force when it was in tension. This meant that the assistor spring was not physically attached to the axle and could come away from it.

As with the relaxation and recovery model in the leaf spring, all of the points in the model of the assistor springs would be in equilibrium. The sum of the forces developed at point Y_4 in the model would therefore be zero. The forces developed by the springs, K_{AS}, K_{AShigh} and K_{ASrr}, were summed, the resulting force being that developed by the damper D_{AS}. As with the relaxation and recovery element in the leaf-spring model, a look-up table was used to derive the damper velocity corresponding to the impressed force, this velocity being integrated to give the nominal assistor spring displacement, Y_4. The displacement of the point Y_5 was found in the same way as that in the leaf-spring relaxation and recovery model, which was of finding the force on the non-linear damper D_{ASrr} due to spring K_{ASrr} and integrating the derived velocity. The characteristics of spring K_{AShigh} were derived from spring K_{AS}, in that the spring generated the same compressive forces as K_{AS}, but in only one tenth of the compression distance (effectively making $K_{AShigh} = 10*K_{AS}$) and thereby enabling the desired non-linearities of this spring to be exercised during compression of the assistor spring.

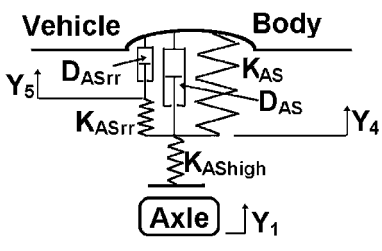

Fig. 10 Assistor-spring model

4.2.2 Assistor-spring model implementation

The assistor-spring model was implemented as shown in the block diagram in Fig. 11. The damping generated by the damping element D_{AS} was non-linear and was deflection-dependent. Thus the force exerted on the damper was divided by the damping at that particular deflection (input U2 divided by input U1 in the 'operator' block), this damping (D_{AS}) being derived with the use of a look-up table with the deflection Y_4 as the input. The stiffness of the spring K_{AS} was, in tension, equal in value but opposite in sense to that of compression.

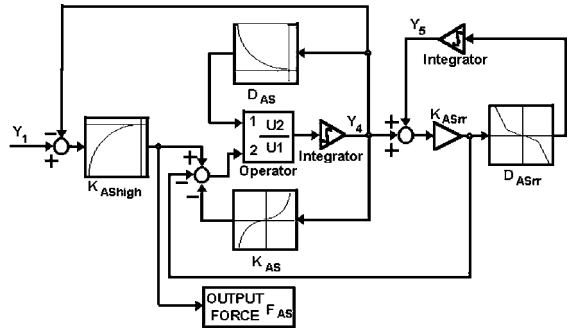

Fig. 11 Assistor-spring block diagram

4.3 Shock absorbers

The shock absorbers (viscous dampers) were included in the model as a viscous damper in series with a compliant bush, and were modelled in a similar manner to that shown in Fig. 9. Both the damping and the spring elements were derived from look-up tables (see Figs 6e and 6f), the damping being a plot of velocity against force, the input to the look-up table being the force and the output being the velocity associated with this force. The integrator would then derive the displacement of the damper piston against which the input displacement (displacement across the suspension) would be compared. The bush force could then be calculated by multiplying the bush compression (or extension) by its stiffness. In this fashion, a system could be made to generate a viscous damping dominated output (and therefore a system dominated by the velocity across the system), even though the input to the model was a displacement.

4.4 Vehicle model

The suspension model so far developed was included in a relatively simple 5 DoF model of the vehicle, the freedoms being the vertical displacement of the body, engine and front and rear axles, and the pitch displacement of the body. Tyre stiffnesses were measured on the real vehicle, lumped masses were used to represent the axles and engine, and a lumped mass with pitch inertia was used to represent the vehicle body. The same types of tests that were carried out on the real vehicle were simulated with the model, to ensure that the model was subjected to as near as possible the same input conditions as the real vehicle. Thus the vehicle tie-down (or 'strop') and axle stands that were used to measure the static stiffnesses were incorporated in the model, and all the measurements taken from the model were the same as those taken on the real vehicle.

The general arrangement of the model is shown in Fig. 12, with the vehicle tie-down strop and axle stand being shown at the front. The springs shown for the suspension incorporate the leaf-spring and assistor spring models developed earlier. The dampers (conventional shock absorbers) shown in the model were derived from look-up tables based on the manufacturer's data (see section 4.3).

4.4.1 Equations of motion

The equations of motion for the vehicle model were developed as follows. The vertical (or bounce) equation of motion for the vehicle body was given by

$$M_b \ddot{y}_b = F_{sf} + F_{sr} + F_{ax} + F_{st} + F_e + M_b g \tag{10}$$

and the pitch equation of motion for the vehicle body was given by

$$I_b \ddot{\Theta}_b = F_{sf} L_f + F_{sr} L_r + F_{ax} L_{ax} + F_{st} L_{st} + F_e L_e \tag{11}$$

where F_{sf} and F_{sr} were the front and rear suspension forces generated by the leaf springs, assistor springs and shock absorbers, such that

$$\begin{aligned} F_{sr} &= F_{suspr} + F_{asr} + F_{Shockr} + Rear\_susp\_F \\ &= (F_{kr} + F_{rrr}) + F_{asr} + F_{Shockr} \\ &\quad + Rear\_susp\_F \end{aligned} \tag{12}$$

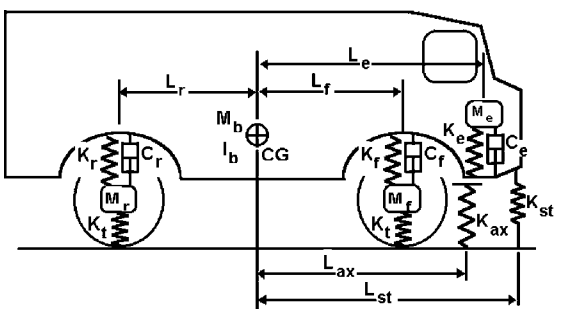

Fig. 12 Vehicle model

and similarly for the front, but excluding the assistor spring forces F_{asf}. The force *Rear_susp_F* was the static load in the suspension due to gravity, the equivalent static load also being present in the front suspension. The front and rear axle equations of motion were given respectively by

$$\begin{aligned} M_f \ddot{y}_{mf} &= -F_{sf} - (y_f - y_{gf})K_t \\ &\quad + Front\_tyre\_load \end{aligned} \tag{13}$$

$$\begin{aligned} M_r \ddot{y}_{mr} &= -F_{sr} - (y_r - y_{gr})K_t \\ &\quad + Rear\_tyre\_load \end{aligned} \tag{14}$$

The equation of motion for the engine was given by

$$M_e \ddot{y}_e = F_e \tag{15}$$

where

$$\begin{aligned} F_e &= [y_e - (y_b + \Theta_b L_e)]K_e \\ &\quad \times [\dot{y}_e - (\dot{y}_e + \dot{\Theta}_b L_e)]C_e + Eng\_susp\_F \end{aligned} \tag{16}$$

The load *Eng_susp_F* was the static load in the engine mounts.

The force generated by the axle stand, F_{ax}, was given by

$$F_{ax} = -(y_b + \Theta_b L_{ax})K_{ax} \tag{17}$$

with the provision that this force could only be positive; i.e. it could only push the vehicle upwards. The force generated by the vehicle tie-down strop, F_{st}, was generated by

$$F_{st} = -(y_b + \Theta_b L_{st})K_{st} \tag{18}$$

with the provision that this force could only be negative; i.e. it could only be in tension and pull the vehicle downwards. The deflection and velocity across the front suspension, *Susp_disp_F* and *Susp_vel_F* were given by

$$Susp\_disp\_F = y_b + \Theta_b L_f - y_f \tag{19}$$

$$Susp\_vel\_F = \dot{y}_b + \dot{\Theta}_b L_f - \dot{y}_f \tag{20}$$

and similarly for the rear suspension, these values being used as inputs into the suspension models described earlier in the paper (sections 4.1, 4.2 and 4.3).

5 THEORETICAL PREDICTIONS

The results from the theoretical predictions of the suspension characteristics, and of the rubber assistor springs, are discussed below. All of the data used in the simulations are presented in Table 1 and Fig. 6.

5.1 Suspension stiffnesses

The vehicle model was used to simulate the same tests that the real vehicle had been subjected to. The results were presented in a similar format to those of the experimental results. The front and rear static suspension stiffness results are presented in Figs 13 and 14.

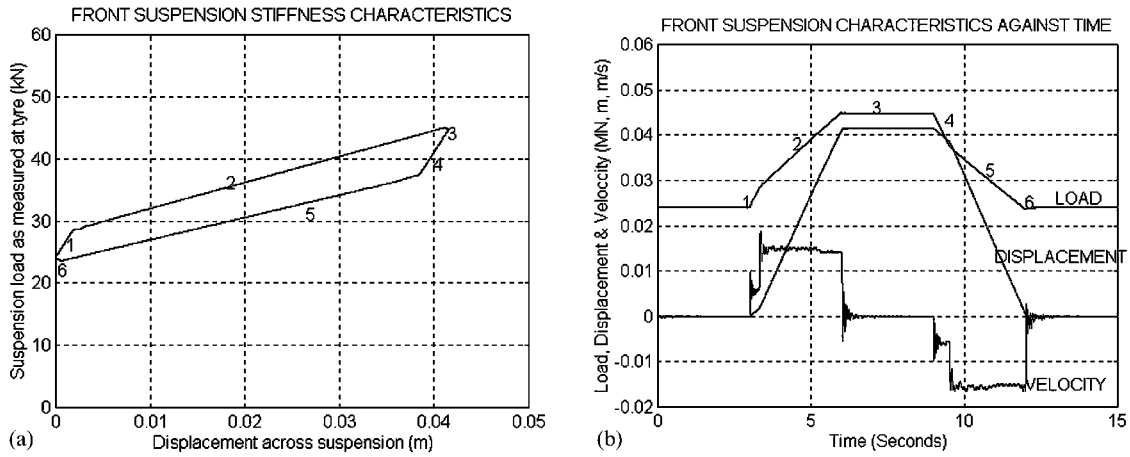

Fig. 13 (a) Theoretical front static suspension stiffness and (b) theoretical front stiffness time histories

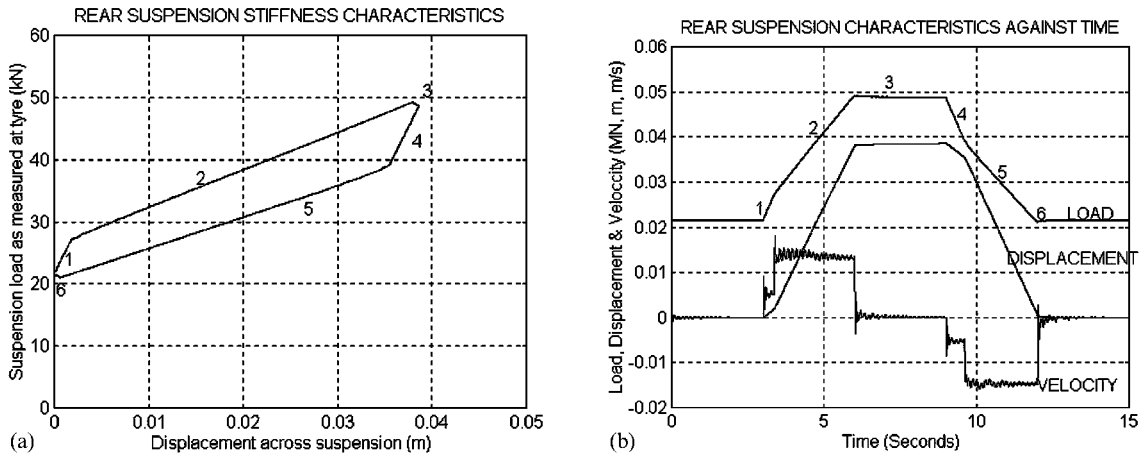

Fig. 14 (a) Theoretical rear static suspension stiffness and (b) theoretical rear stiffness time histories

Examination of these theoretical predictions showed that the suspension model was capable of simulating the same basic characteristics as the real suspension. Again, six regimes were identified, these being the high and low stiffness regions (regimes 1 and 4 and 2 and 5 respectively) and the relaxation and recovery regions when the suspension was held at constant deflection after a change in deflection had occurred (regimes 3 and 6 respectively).

Small discrepancies between the theoretical predictions and the experimental results were evident, however, particularly in the amount of hysteresis in the force against deflection loops. It is thought that these were likely to be due to the characteristics of the rubber assistor springs under the non-dynamic compression test conditions and to other variables not included in the model (drive line stiffness, etc.).

The time histories of the suspension load, deflection and velocity also showed very similar characteristics to those of the real suspension.

5.2 Assistor springs

The simulation results of the assistor-spring model were plotted on the same graph as the experimental data (Fig. 5). The theoretical predictions followed the experimental curve accurately for most of the deflection range; only at very small deflections were any discrepancies evident.

The predicted effects of the assistor springs on the suspension stiffness characteristics were similar to those of the real suspension. The assistor springs had the effect of increasing the difference between the loading and unloading regions of the stiffness curves, this being due to the increase in the degree of relaxation and recovery in the suspension. However, as noted above, the static nature of the actual suspension stiffness measurements compared to the dynamic measurement data of the assistor springs meant that the small discrepancies noted above were probably due in large part to incomplete data concerning the behaviour of the assistor springs.

5.3 Model implications

The model so far developed made predictions that compared well with the experimental data for a single loading and unloading cycle. If, however, the suspension model were to be loaded and unloaded in a series of steps, then

the model would predict that only when a change of direction occurred would the high stiffness regime manifest itself. This would be due to the fact that at the end of any one loading or unloading step, the high stiffness spring would be in a state of compression or tension to the point where any further change in load in the same direction would immediately overcome the resistive forces to further deflection created by the friction plates and the low stiffness spring. Thus only when a change of direction occurred would the high stiffness spring first have to be loaded or unloaded from one state (compression or tension) to the other, with the change in load required to achieve the breakaway force in the new direction being twice that generated by the product of the load acting on the friction plates and the effective coefficient of friction between these plates.

The model was used to simulate the suspension as it was loaded up in a series of six steps from zero load. Upon reaching the maximum deflection, the suspension was briefly held and then unloaded back to zero in a series of five steps. The results from this test are shown in the usual format in Fig. 15. The loading and unloading portions of the load against deflection curve followed basically the same straight lines. Only when the direction of deflection changed did the high stiffness regime manifest itself. The loading and unloading curves show evidence of relaxation and recovery respectively whenever the deflection was held constant at the end of each step. Furthermore, the effect of the assumed zero value of preload [P_0 in equation (6)] can be seen as the converging loading and unloading portions of the loop in Fig. 15a as the load approached zero.

The results from a similar test on the real vehicle are shown in Fig. 16. The front suspension was loaded up in six steps from zero, held and then unloaded in five steps. The loading and unloading regions of the load against deflection curve can be seen to have followed a straight line in each case, with evidence of relaxation and recovery being observed at the end of each step. The high stiffness regime only manifested itself when a change of direction of the suspension deflection occurred. These results are exactly as predicted by the model. Also evident is the fact that the loading and unloading portions of the loop in Fig. 16a do not converge at zero load. This would be due to the existence of a small, but nevertheless non-zero, preload P_0 existing

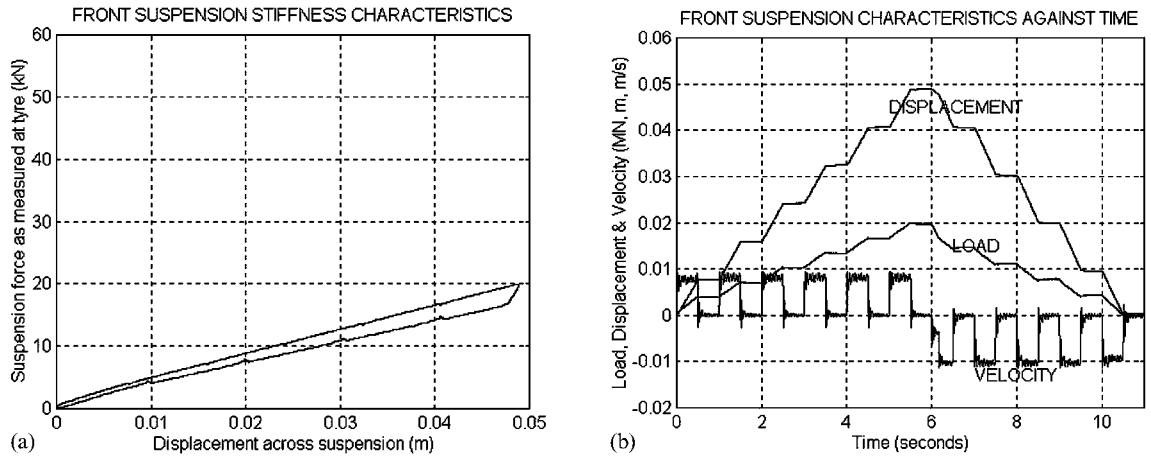

Fig. 15 (a) Theoretical step loading static stiffness and (b) theoretical step loading stiffness time histories

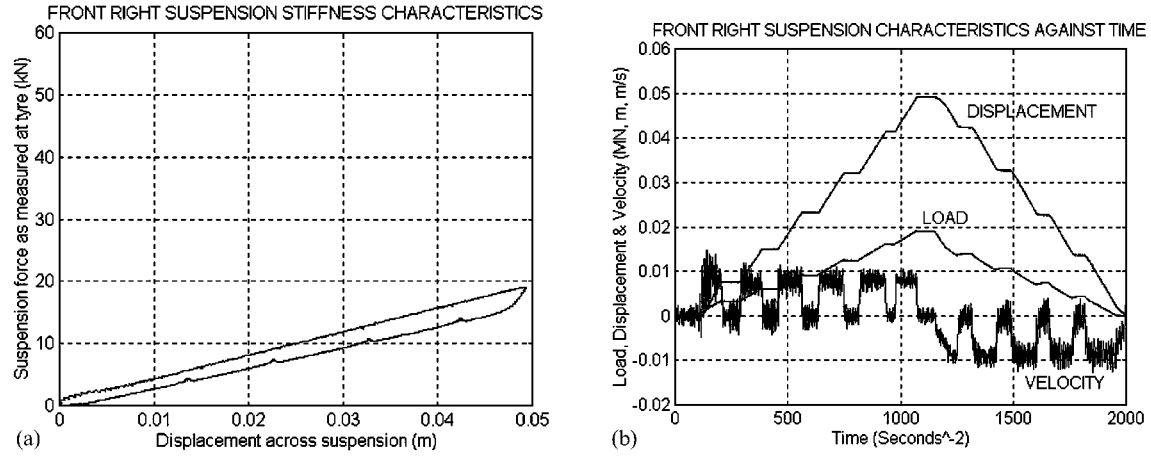

Fig. 16 (a) Experimental step loading static stiffness and (b) experimental step loading stiffness histories

between the leaf springs. The ratio between the low and high stiffness regimes, being on the order of 5.5 (Table 3), did not suggest any simple form of beam bending mechanism for the high stiffness regime. Furthermore, the model also assumed that kinetic friction (friction during movement) was the same as static friction in both directions.

5.4 Dynamic model predictions

Thus far, the models created have been able to simulate the static stiffness characteristics of the leaf spring suspension, the hysteresis relaxation and recovery effects of the suspension after a change in load and deflection had taken place and the stiffness and damping effects of the assistor springs. With the assumption that the dynamic friction effects were the same as the static friction effects, the acceleration transmissibility frequency responses of the sprung and unsprung masses predicted by the model were compared to those obtained from the actual vehicle.

As noted in section 2.1.3, linear undamped predictions for the sprung and unsprung natural frequencies (1.95 and 10.8 Hz respectively) were different from those measured experimentally (2.44 and 19 Hz). Furthermore, it was established that although the linear 5 DoF state-variable model was able to predict the sprung and unsprung mass resonant frequencies (1.9 Hz using the low stiffness regime and 17 Hz using the high stiffness regime respectively), it could only do this over a limited range of frequencies, and it completely failed to capture the transition between the low and high stiffness regimes within one single frequency sweep. As it was the effects of the friction between the leaves that gave rise to the static non-linear characteristics of the springs, if the vehicle model was able to predict similar dynamic results to those measured experimentally, and in particular capture the transition from the high deflection low stiffness regime at low frequencies to the low deflection high stiffness regime at high frequencies during a single frequency sweep, it could reasonably be concluded that the non-linear model was able to successfully simulate the principal dynamic characteristics of the vehicle suspension. Furthermore, it would also provide good evidence justifying the assumption that dynamic friction was effectively the same as static friction.

5.4.1 Frequency response predictions

The model thus developed was subjected to a frequency analysis of a very similar nature to that of the actual vehicle. A sine wave vertical displacement was input into the tyres to simulate the experimental hydraulic actuators, the frequency being increased in a number of discrete steps. For each step, a number of cycles were input into the vehicle model and the steady state response of the model recorded. A fast Fourier transform (FFT) algorithm was used to determine the various acceleration amplitudes of the vehicle response, which were compared to the acceleration amplitude of the input to determine the sprung and unsprung acceleration transmissibility ratios for each frequency. As with the experimental procedure, the displacement input amplitude was decreased at a rate of 2 dB/octave above 2 Hz and the starting amplitude was 5 mm. The acceleration transmissibility ratios were then plotted against frequency on a suitable log graph to enable direct comparison of the experimentally derived frequency responses to those predicted by the model.

The results of the theoretical frequency analyses are shown in Fig. 17a (sprung mass) and Fig. 17b (unsprung masses). A number of curves are shown in Fig. 17a, three of these being the response of the vehicle body front, centre of gravity and rear (marked 'F', 'CG' and 'R' respectively), and correspond to the three experimentally derived curves shown in Fig. 2a. Another curve is shown in Fig. 17a, which is the response of the engine (marked 'Engine').

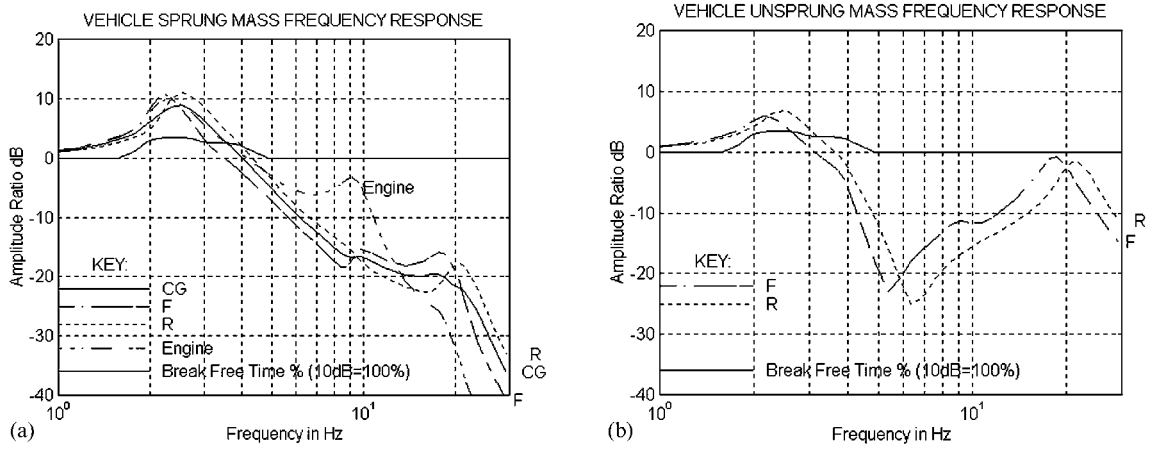

Fig. 17 (a) Theoretical sprung mass frequency responses and (b) theoretical unsprung mass frequency response

Comparison of the frequency response predictions in Fig. 17 with those of the actual vehicle in Fig. 2 revealed that the predictions of the non-linear model were extremely good, far better in fact than the linear damped 5 DoF state-variable model. At 2.4 Hz, the predicted bounce (sprung mass) resonant frequency matched almost exactly the experimental results (2.44 Hz). A similarly good correlation was obtained for the unsprung mass resonant frequencies (20 Hz predicted compared to 19 Hz). Furthermore, the amplitude ratios for the sprung and unsprung mass resonant frequencies were almost identical. The model was certainly able to capture the transition from the low stiffness regime at the bounce frequency to the high stiffness regime above about 4 Hz.

Figures 17a and b also show a curve marked 'Break Free Time %'. This curve was a measure of how long during any particular sine wave cycle at any particular frequency the suspension deflected sufficiently for it to act as normal leaf springs (not locked together). This curve was plotted against the vertical dB scale, such that 100 per cent break-free time equalled 10 dB and 50 per cent equalled 5 dB. The curve shows that even at the sprung mass resonant frequency, the maximum amount of time that the suspension was acting as normal leaf springs was only 35 per cent; for the remaining time the suspension leaves were in their locked state. Above 5 Hz, the leaves were permanently locked together, which would account for the apparent success of the linear 5 DoF state-variable model in predicting the shape of the frequency response curves when using the higher suspension stiffness regime. The partial breakaway state of the springs would also account for the actual resonant frequency of the sprung mass being between the two 5 DoF state-variable predictions for this frequency, as the two stiffness regimes would be to some extent averaged to produce an intermediate stiffness that resulted in the actual resonant frequency measured.

Also worth noting was that the curve marked 'F' (vehicle front) in Fig. 2a experienced an unusual feature between 9 and 11 Hz, and this was again shown to be present in the equivalent curve in Fig. 17a and the 5 DoF state-variable predictions. This feature was caused by the bounce resonant frequency of the engine on its resilient mounts.

5.4.2 *Effect of rubber bushed shock absorbers*

The results so far generated, both experimentally and theoretically, were compared in Table 4. They show that the non-linear suspension model developed in this paper was able to predict the resonant frequencies of the vehicle accurately. However, the linear 5 DoF state-variable model makes predictions for the unsprung mass resonant frequencies that are too low, irrespective of which suspension stiffness regime was used. Clearly some other spring element is acting on the unsprung masses to raise their resonant frequencies. The non-linear model has been used to show that this influence was mostly due to the compliant rubber bushes that were incorporated at each end of the suspension shock absorbers (viscous dampers, see section 4.3).

If these shock absorbers were included in the non-linear model as only their non-linear viscous damping element, the resulting unsprung mass resonant frequencies would be much closer to those predicted by the high stiffness regime linear 5 DoF state-variable model, as shown by rows 5 and 3 respectively in Table 4 (see also Figs 18a and b for the frequency responses). Although as a first approximation these rubber bushes might be considered insignificant, their actual effect was to raise the unsprung mass resonant frequencies by approximately 2.4 Hz. The remaining discrepancies between the predicted resonant frequencies and what could be accounted for solely by a combination of suspension stiffnesses were probably due to a slight underestimate of the unsprung masses, which would serve to raise these frequencies in the non-linear model above what they would otherwise be in practice.

5.4.3 *Leaf-spring suspension ride characteristics*

The results in Table 4 also show that the sprung mass resonant frequency was determined by a combination of both the low and high stiffness regimes of the leaf springs. Furthermore, the unsprung mass resonant frequencies were dominated by the high stiffness regime, and other effects (rubber bushed shock absorbers, rubber bump stops, etc.) served to raise their resonant frequencies still higher.

For good ride quality, the sprung mass resonant

Table 4 Experimental and theoretical results

Condition		Sprung mass resonant frequency and amplitude ratio	Unsprung mass resonant frequency and amplitude ratio	Results derived from
1	Experimental results	2.4 Hz and 10.24 dB	19 Hz and 1 dB	Experiment
2	Low suspension stiffness regime	1.9 Hz and 13.5 dB	10.8 Hz and 4.5 dB	Linear 5 DoF
3	High suspension stiffness regime	2.8 Hz and $\gg$20 dB	17.0 Hz and -2 dB	Linear 5 DoF
4	Low and high stiffness regimes, shock absorbers with rubber bushes	2.4 Hz and 8.5 dB	20.0 Hz* and -1 dB	Non-linear model
5	Low and high stiffness regimes, shock absorbers without bushes	2.4 Hz and 8.5 dB	17.6 Hz* and -5 dB	Non-linear model

* Average of front and rear unsprung masses.

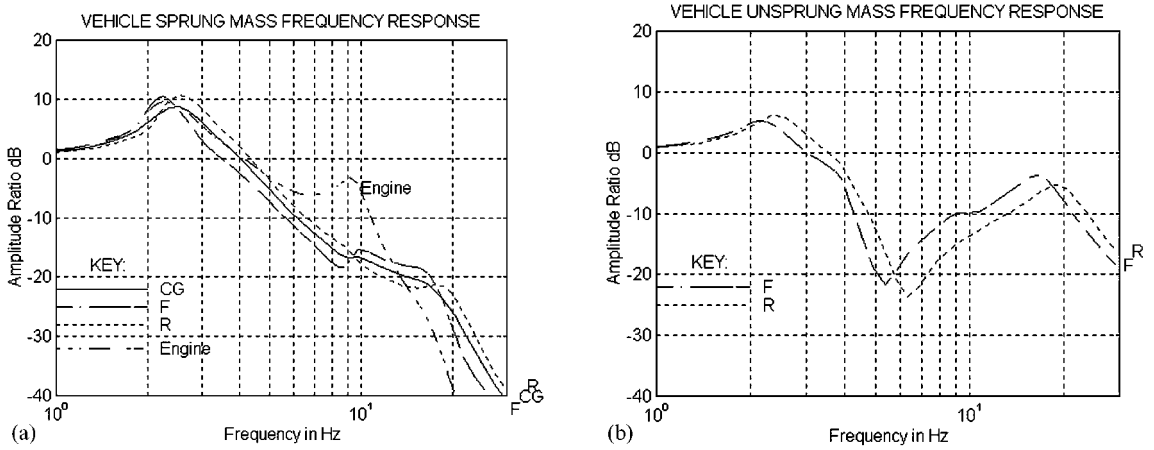

Fig. 18 (a) Theoretical sprung mass frequency responses and (b) theoretical unsprung mass frequency response for shock-absorbers without compliance

frequency would ideally be between 1.5 and 2 Hz, with the unsprung mass resonant frequencies being about 10 Hz. The damping would be set to allow adequate control of the amplitude ratios of these resonances.

A comparison of the linear 5 DoF predictions with the non-linear equivalent in Table 4 suggests that the leaf springs had the effect of not only increasing the sprung mass resonant frequency from 1.9 to 2.4 Hz (an undesirable effect) but also of decreasing very significantly the amplitude ratio of this resonance, from 13.5 to 8.5 dB. Indeed, calculations show that this was equivalent to having four times as many shock absorbers on the vehicle. Whereas this reduction in amplitude ratio at the sprung mass resonant frequency was a desirable effect, it had been achieved at the expense of riding on a near solid suspension (high stiffness regimes) under most normal road conditions, and the apparent advantages were therefore offset by a harsher ride quality with increased road noise and structural vibration. This latter point was certainly borne out by the available evidence, as the vehicle was generally regarded as being very noisy and tiring to drive.

6 CONCLUSIONS

The following are conclusions:

1. The frequency response characteristics of a 10 ton truck with multiple-leaf suspension springs has been investigated and found to have resonant frequencies that differed markedly from what might be expected from linear 5 DoF state-variable model predictions of the system.
2. A non-linear model of the vehicle and its suspension has been created that was able to predict accurately the static stiffness and hysteresis characteristics of the leaf spring suspension system, in particular the two distinct stiffness regimes of the leaf springs.
3. Furthermore, the model was able to predict accurately the dynamic frequency response characteristics of the vehicle suspension system, particularly the transition from the high deflection–low suspension stiffness regime at the sprung mass resonant frequency, to the low deflection–high stiffness regime at all frequencies above 4 Hz, the latter including the unsprung mass resonant frequencies.
4. The model's assumption that the static and dynamic elements of the suspension friction characteristics were equal was supported by the available evidence.
5. The sprung mass resonant frequency was derived from a combination of both stiffness regimes of the leaf springs, whereas the unsprung mass resonant frequencies were dominated by the friction-induced locked-leaf state (higher stiffness regime) of the suspension leaves.
6. Even apparently insignificant suspension elements are necessary to predict correctly the vehicle resonant frequencies (shock absorber rubber bushes, assistor springs).
7. Such non-linear stiffness characteristics can result in the vehicle riding on a near-solid suspension under most normal road conditions, with consequent increased levels of road noise and vehicle vibration.

REFERENCES

1 **Potter, T. E. C., Cebon, D.** and **Cole, D. J.** Indirect methods for assessing road friendliness of lorry suspensions. *Proc. Instn Mech. Engrs, Part D: J. Automobile Engineering*, 1997, **211**(D4), 243–256.
2 **Winkler, C. B.** and **Hagan, F.** A test facility for the measurement of heavy vehicle suspension parameters. SAE paper 800906, 1980.
3 **Haessig, D. A.** and **Friedland, B.** On the modelling and simulation of friction. *Trans. ASME, J. Dynamic Systems, Measmt and Control*, 1991, **113**.

4 **Wong, J. Y.** *Theory of Ground Vehicles*, 1993 (Wiley–Interscience, New York).
5 **Fancher, P. S.**, *et al.* Measurement and representation of the mechanical properties of truck leaf springs. SAE paper 800905, 1980.
6 **Lindley, P. B.** Engineering design with natural rubber. NR Technical Bulletin, Malayan Rubber Fund Board, Natural Rubber Producers Research Association, 1966.

APPENDIX

Linear damped 5 degree-of-freedom state-variable model of suspension

The vehicle suspension system and principal dynamic components can be modelled as a linear spring mass damper system that lends itself readily to analysis using state-variable techniques within MATLAB. The system is shown in Fig. 19, and the equations of motion are presented below. The tie-down strop and axle stand are ignored.

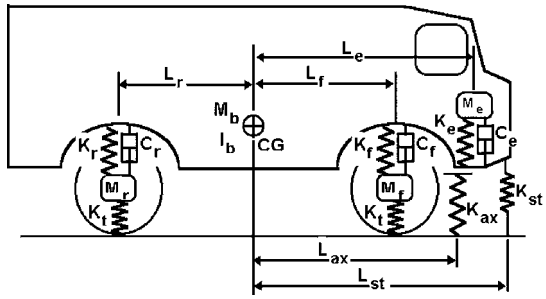

Fig. 19 Linear damped 5 DoF representation of the vehicle suspension

Body (sprung mass) vertical motion:

$$\ddot{y}_b M_b = (y_f - y_b - \theta_b L_f)K_f + (y_r - y_b - \theta_b L_r)K_r + (y_e - y_b - \theta_b L_r)K_e + (\dot{y}_f - \dot{y}_b - \dot{\theta}_b l_f)C_f + (\dot{y}_r - \dot{y}_b - \dot{\theta}_b L_r)C_r + (\dot{y}_e - \dot{y}_b - \dot{\theta}_b L_r)C_e \quad (21)$$

Body (sprung mass) angular pitch motion:

$$\ddot{\theta}_b I_b = (y_f - y_b - \theta_b L_f)L_f K_f + (y_r - y_b - \theta_b L_r)L_r K_r + (y_e - y_b - \theta_b L_r)L_e K_e + (\dot{y}_f - \dot{y}_b - \dot{\theta}_b l_f)L_f C_f + (\dot{y}_r - \dot{y}_b - \dot{\theta}_b L_r)L_r C_r + (\dot{y}_e - \dot{y}_b - \dot{\theta}_b L_r)L_e C_e \quad (22)$$

Front axle (unsprung mass):

$$\ddot{y}_f M_f = (y_b + \theta_b L_f - y_f)K_f + (\dot{y}_b + \dot{\theta}_b L_f - \dot{y}_f)C_f + (y_g - y_f)K_t \quad (23)$$

Rear axle (unsprung mass):

$$\ddot{y}_r M_r = (y_b + \theta_b L_r - y_r)K_r + (\dot{y}_b + \dot{\theta}_b L_r - \dot{y}_r)C_r + (y_g - y_r)K_t \quad (24)$$

where y_g in equations (23) and (24) is the ground displacement system excitation input to the wheels.

Engine:

$$\ddot{y}_e M_e = (y_b + \theta_b L_e - y_e)K_e + (\dot{y}_e + \dot{\theta}_e L_e - \dot{y}_e)C_e \quad (25)$$

These equations can be written as a set of first-order differential equations and then represented in state-variable form as the vector equation:

$$\dot{\boldsymbol{x}} = f(\boldsymbol{x}, \boldsymbol{u}) \quad (26)$$

where the input is $\boldsymbol{u}$ and the output is

$$\boldsymbol{y} = h(\boldsymbol{x}, \boldsymbol{u}) \quad (27)$$

For the linear case, equations (26) and (27) can be written as

$$\dot{\boldsymbol{x}} = \mathbf{F}\boldsymbol{x} + \boldsymbol{G}\boldsymbol{u} \quad (28)$$

and

$$\boldsymbol{y} = \mathbf{H}\boldsymbol{x} + J\boldsymbol{u} \quad (29)$$

where for an nth-order system, $\mathbf{F}$ is an $n \times n$ system matrix (in this case $n = 10$), $\boldsymbol{G}$ is an $n \times 1$ column vector of inputs, $\mathbf{H}$ is an $m \times n$ output matrix and J is a scaler called the direct transmission term. For the 5 DoF system represented by Fig. 19 and equations (21) to (25), and ignoring the effects of gravity, matrices $\mathbf{F}$, $\mathbf{G}$, $\mathbf{H}$ and $\mathbf{J}$ for this system are as follows:

System matrix **F**:

$$\mathbf{F}_{\text{row1}} = [0, 1, 0, 0, 0, 0, 0, 0, 0, 0]$$

$$\mathbf{F}_{\text{row2}} = \left[-\frac{K_\text{f} + K_\text{r} + K_\text{e}}{M_\text{b}}, -\frac{C_\text{f} + C_\text{r} + C_\text{e}}{M_\text{b}}, -\frac{L_\text{f}K_\text{f} + L_\text{r}K_\text{r} + L_\text{e}K_\text{e}}{M_\text{b}}, -\frac{L_\text{f}C_\text{f} + L_\text{r}C_\text{r} + L_\text{e}C_\text{e}}{M_\text{b}}, \frac{K_\text{f}}{M_\text{b}}, \frac{C_\text{f}}{M_\text{b}}, \frac{K_\text{r}}{M_\text{b}}, \frac{C_\text{r}}{M_\text{b}}, \frac{K_\text{e}}{M_\text{b}}, \frac{C_\text{e}}{M_\text{b}} \right]$$

$$\mathbf{F}_{\text{row3}} = [0, 0, 0, 1, 0, 0, 0, 0, 0, 0]$$

$$\mathbf{F}_{\text{row4}} = \left[-\frac{L_\text{f}K_\text{f} + L_\text{r}K_\text{r} + L_\text{e}K_\text{e}}{I_\text{b}}, -\frac{L_\text{f}C_\text{f} + L_\text{r}C_\text{r} + L_\text{e}C_\text{e}}{I_\text{b}}, -\frac{L_\text{f}^2K_\text{f} + L_\text{r}^2K_\text{r} + L_\text{e}^2K_\text{e}}{I_\text{b}}, -\frac{L_\text{f}^2C_\text{f} + L_\text{r}^2C_\text{r} + L_\text{e}^2C_\text{e}}{I_\text{b}}, \frac{L_\text{f}K_\text{f}}{I_\text{b}}, \frac{L_\text{f}C_\text{f}}{I_\text{b}}, \frac{L_\text{r}K_\text{r}}{I_\text{b}}, \frac{L_\text{r}C_\text{r}}{I_\text{b}}, \frac{L_\text{e}K_\text{e}}{I_\text{b}}, \frac{L_\text{e}C_\text{e}}{I_\text{b}} \right]$$

$$\mathbf{F}_{\text{row5}} = [0, 0, 0, 0, 0, 1, 0, 0, 0, 0]$$

$$\mathbf{F}_{\text{row6}} = \left[\frac{K_\text{f}}{M_\text{f}}, \frac{C_\text{f}}{M_\text{f}}, \frac{L_\text{f}K_\text{f}}{M_\text{f}}, \frac{L_\text{f}C_\text{f}}{M_\text{f}}, -\frac{K_\text{f} + K_\text{t}}{M_\text{f}}, -\frac{C_\text{f}}{M_\text{f}}, 0, 0, 0, 0 \right]$$

$$\mathbf{F}_{\text{row7}} = [0, 0, 0, 0, 0, 0, 0, 1, 0, 0]$$

$$\mathbf{F}_{\text{row8}} = \left[\frac{K_\text{r}}{M_\text{r}}, \frac{C_\text{r}}{M_\text{r}}, \frac{L_\text{r}K_\text{r}}{M_\text{r}}, \frac{L_\text{r}C_\text{r}}{M_\text{r}}, 0, 0, -\frac{K_\text{r} + K_\text{t}}{M_\text{r}}, -\frac{C_\text{r}}{M_\text{r}}, 0, 0 \right]$$

$$\mathbf{F}_{\text{row9}} = [0, 0, 0, 0, 0, 0, 0, 0, 0, 1]$$

$$\mathbf{F}_{\text{row10}} = \left[\frac{K_\text{e}}{M_\text{e}}, \frac{C_\text{e}}{M_\text{e}}, \frac{L_\text{e}K_\text{e}}{M_\text{e}}, \frac{L_\text{e}C_\text{e}}{M_\text{e}}, 0, 0, 0, 0, -\frac{K_\text{e}}{M_\text{e}}, -\frac{C_\text{e}}{M_\text{e}} \right]$$

The input matrix **G** is given by

$$\boldsymbol{G} = \left[0, 0, 0, 0, 0, \frac{K_\text{t}}{M_\text{f}}, 0, \frac{K_\text{t}}{M_\text{r}}, 0, 0 \right]^\text{T}$$

The output matrix **H** derives the displacement responses of the five individual degrees of freedom and the displacement of the vehicle body at the positions of the front and rear mounted experimental test accelerometers at distances L_accelf and L_accelr from the body centre of gravity respectively, giving seven outputs in total:

$$\mathbf{H} = \begin{bmatrix} 1, 0, 0, 0, 0, 0, 0, 0, 0, 0 \\ 0, 0, 1, 0, 0, 0, 0, 0, 0, 0 \\ 0, 0, 0, 0, 1, 0, 0, 0, 0, 0 \\ 0, 0, 0, 0, 0, 0, 1, 0, 0, 0 \\ 0, 0, 0, 0, 0, 0, 0, 0, 1, 0 \\ 1, 0, L_\text{accelf}, 0, 0, 0, 0, 0, 0, 0 \\ 1, 0, L_\text{accelr}, 0, 0, 0, 0, 0, 0, 0 \end{bmatrix}$$

Matrix **J** is given by a (7×1) column vector of zeros.

The frequency responses of the system-to-ground inputs were derived using MATLAB. Two sets of results were generated; the first (shown in Figs 20a and b for the sprung and unsprung masses respectively) assumed that the suspension stiffness was given by the nominal stiffness of the suspension leaf springs (sum of the stiffnesses of the individual leaves) and the second (shown in Figs 21a and b) assumed that the suspension stiffness was in a locked-up state, thereby giving a much higher suspension stiffness. The resonant frequencies of the sprung and unsprung masses for the two different stiffness values are given in Table 5.

It is clear from the two sets of graphs and Table 5 that the stiffness of the suspension makes a dramatic difference to the response of the vehicle body and the axles. The response of the engine is largely insensitive to that of the rest of the system. All of the data used in these predictions is presented in Table 1 and Fig. 6, and the two stiffness regimes

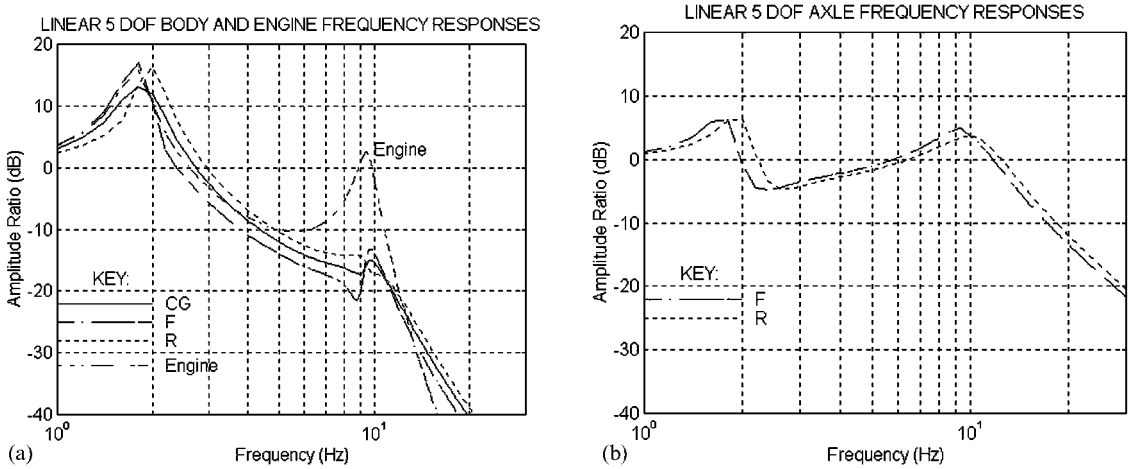

Fig. 20 (a) Sprung mass frequency responses and (b) unsprung mass frequency responses for nominal suspension stiffness

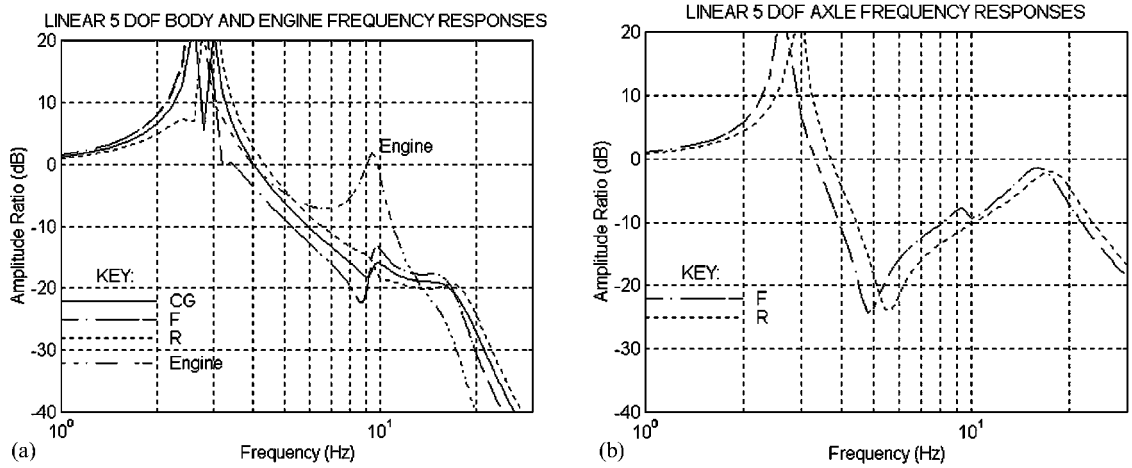

Fig. 21 (a) Sprung mass frequency responses and (b) unsprung mass frequency responses for 'locked leaf' suspension stiffness

Table 5 Lumped mass resonant frequencies

Lumped mass	Low suspension stiffness resonant frequency and amplitude ratio	High suspension stiffness resonant frequency and amplitude ratio
1 Vehicle body centre of gravity	1.9 Hz and 13.5 dB	2.8 Hz* and $\gg$20 dB
2 Engine	9.3 Hz	9.3 Hz
3 Front and rear axles (average)	9.5 Hz and 4.5 dB	17 Hz and -2 dB

* Average of the two peaks.

were as follows:

$K_f = K_{Lowf}$ (low stiffness regime) and $5.5K_{Lowf}$ (high stiffness regime)

$K_r = K_{Lowr}$ (low stiffness regime) and $5.5K_{Lowr}$ (high stiffness regime)